

Systems Development of a Two-Axis Stabilised Platform to Facilitate Astronomical Observations from a Moving Base

James H. Hepworth
Department of Mechanical Engineering
University of Cape Town
Cape Town, South Africa
james.hepworth@alumni.uct.ac.za

Abstract—This project aimed to design, simulate, and implement a two-axis inertially stabilised platform (ISP) for use in astronomical applications. It aimed to approximate the stabilisation of a Meade ETX-90 3.5" compound telescope at low-cost using a mechanical assembly designed to geometrically and inertially model the telescope. A set of system specifications was developed to guide design decisions and to provide an analysis framework against which the performance of the implemented system was compared. During the project, the electro-mechanical structure of the ISP was designed and implemented, the associated electrical systems were specified and configured, an image processing script capable of detecting and locating the centre of the Moon in a camera field-of-view was written, a complete simulation model for the system was developed and used to design various classical controllers for the ISP control system. These controllers were implemented on a STM32F051 microcontroller tasked with managing the various control and communications tasks required by the system. Finally, a user interface was written in LabVIEW to facilitate intuitive user control of the system and perform datalogging of the system runtime data. This paper summarises the design and test results of these various systems and shows the correlation between the hardware results and simulated results of the ISP system developed.

Keywords— *Inertial Stabilisation, Control Systems Design, Systems Modelling, Simulation*

I. INTRODUCTION

Many examples of modern electronic and optical systems require inertial stabilisation for them to achieve their maximum performance [1], [2]. Inertially Stabilised Platforms (ISPs) are systems capable of isolating a sensor from its host by attenuating rotational disturbances coupled from the host to the sensor which result in a reduction in the sensor's performance. Some examples of systems whose performance may be improved by using an ISP include missile seeker heads, communications systems, inertial navigation systems, surveillance systems, and optical imaging systems [3]. ISPs aim to control the line-of-sight (LOS) between a sensor and a target. They perform two distinct operations; keeping track of the target as the sensor host and the target move in inertial space and attenuating rotational rate disturbances incurred to the sensor by host vehicle motion.

Observing a celestial object at high magnification through a telescope illustrates the problem clearly; even the smallest rotation of the telescope will cause, at the very least, blurring of the image observed, but is likely to cause a loss of the target altogether from the telescope field-of-view (FOV). Likewise, a high-resolution camera requires the sensor be as still as possible for maximum image clarity to be achieved. This

problem is clearly aggravated when the observation instrument is mounted on a moving host. A telescope affixed to the Earth is also subject to this problem and at high magnification, celestial objects move quickly out of the FOV solely due to the Earth's rotation.

The inclusion of an automatic target tracking and stabilisation control system to a telescope would provide a means to address these problems: If the telescope was accidentally (or intentionally) moved after observations had begun, the system would, within design constraints, keep the target in the centre of the FOV of the sensor. This has several positive implications, including increasing the ease of use of the telescopic system for the amateur astronomer, and allowing for the telescope to be mounted on a moving base such as the deck of a ship or a moving motor vehicle.

This project aimed to implement a stabilised platform and automatic target tracker able to facilitate the control of a Meade ETX-90 telescope to automatically track the Moon from a moving vehicle. Firstly, the main specifications of the system are presented before the design, implementation and tested performance of the ISP are summarised.

II. MAIN SYSTEM SPECIFICATIONS

The following specifications formed part of a broader set of technical design specifications and defined the overall design goals for the ISP system developed.

A. Mechanical Specifications

- i. The system should facilitate the inertial control of a 3.5" telescope.
- ii. The system should allow for motion control about two control axes.
- iii. The total system mass should be limited to a 9 kg.

B. Operational Specifications

- iv. The target tracker should have a tracking error of less than 0.25 mrad.
- v. System jitter should be limited to 2 mrad under dynamic host conditions and 0.5 mrad under static host conditions.

C. Constraints

- vi. Development costs should be less than R5000.00

III. SYSTEMS DEVELOPMENT

This section presents the development of the design of the ISP implemented in this project. The electro-mechanical assembly of the ISP system serves the purpose of mounting, constraining and controlling the motion of the telescope to be stabilised. Two-axis of control were deemed sufficient for the project as rotation of the telescope FOV about its centre was allowable during operation. This section begins with a description of the system kinematics used to model the gimballed mechanism employed by the ISP, before a description of the mechanical, electrical and software systems developed is given.

A. System Model

1) Axes and Angle Definitions

Figure 1 below shows the schematic of the gimballed mechanism used to model the ISP. In the figure, the gimbal facilitates rotation about the z_b, z_g axis whilst the platform rotates about the y_g, y_p axis. Here, the gimbals are modelled as rigid-bodies suspended on frictionless joints, however, later, in the system simulation shown in Section IV, inter-gimbal friction was modelled. The telescope is mounted on the platform. Three reference frames are defined using triads of orthogonal vectors, $\{x, y, z\}$ fixed to their hosts such that the frames rotate with the members to which they are affixed. These frames are defined as:

- i. The Inertial reference frame, I, given by $\{x_i, y_i, z_i\}$,
- ii. The Base fixed frame, B, given by $\{x_b, y_b, z_b\}$,
- iii. The Gimbal fixed frame, G, given by $\{x_g, y_g, z_g\}$, and
- iv. The Platform fixed frame, P, given by $\{x_p, y_p, z_p\}$.

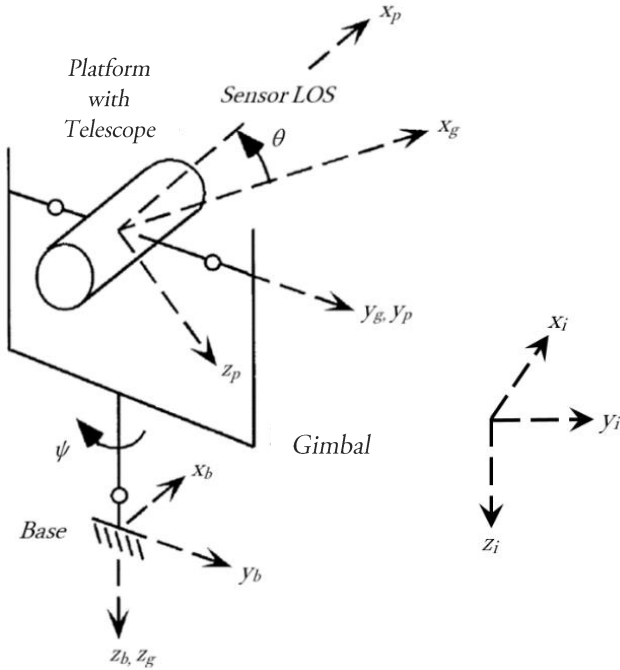


Figure 1: Gimballed mechanism - Adapted from [4]

The angular positions of the frames relative to each other are given by the yaw angle (the angle between frames B and G), ψ , and the pitch angle (the angle between frames G and P), θ . These are shown by Figure 2 below.

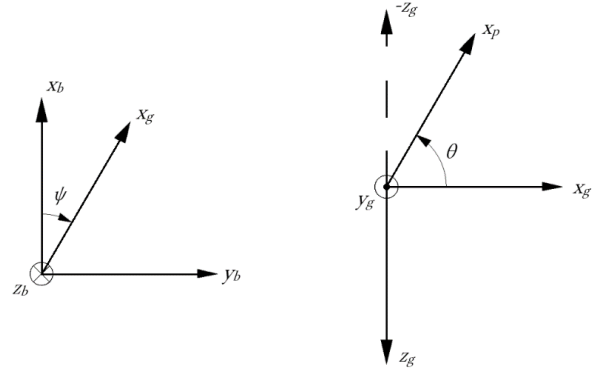


Figure 2: Relative angle definitions

$\dot{\psi}$ is, therefore, the angular rate between the base and the gimbal, and $\dot{\theta}$ is, therefore, the angular rate between the gimbal and the platform. The definitions given above are used to represent a Euler sequence of the order yaw-pitch or ψ - θ , from the base to the platform. Frame B is carried into frame G by a rotation ψ about the z_b, z_g axis such that a vector in frame B may be transformed into frame G using the rotation matrix, L_{GB} , where:

$$\overline{L}_{GB} = \begin{bmatrix} \cos \psi & \sin \psi & 0 \\ -\sin \psi & \cos \psi & 0 \\ 0 & 0 & 1 \end{bmatrix}$$

Frame G is carried into frame P by a rotation θ about the y_g, y_p axis such that a vector in frame G may be transformed into frame P using the rotation matrix, L_{PG} , where:

$$\overline{L}_{PG} = \begin{bmatrix} \cos \theta & 0 & -\sin \theta \\ 0 & 1 & 0 \\ \sin \theta & 0 & \cos \theta \end{bmatrix}$$

2) Kinematic Relationships

This section is heavily drawn from [5], but also draws from [4], [6], and [7]. The general equations of motion for the gimbals of the two-axis system are derived from the law of the conservation of angular momentum:

$$\sum \bar{M} = \dot{\bar{H}} \quad \text{where} \quad \bar{H} = \bar{I} \cdot \bar{\omega} \quad (1)$$

This states that the sum of the external moments, \bar{M} , about a fixed point or the centre of mass of a body is equal to the time derivative of the angular momentum, \bar{H} , of the body where \bar{H} is defined relative to a fixed co-ordinate system and $\bar{\omega}$ is the angular velocity of the body. When the angular momentum vector is defined relative to a moving coordinate system, which has a rotational velocity of $\bar{\Omega}$ the conservation of momentum equation can be modified to include the changes in momentum due to the Coriolis Theorem [8], giving:

$$\sum \bar{M} = \dot{\bar{H}} + \bar{\Omega} \times \bar{H} \quad (2)$$

If the moving coordinate system is attached to the rotating body, $\bar{\Omega} = \bar{\omega}$ and the inertia tensor, \bar{I} , of the body is constant with respect to time, giving:

$$\sum \bar{M} = \bar{I} \cdot \dot{\bar{\omega}} + \bar{\omega} \times \bar{H} \quad (3)$$

The two-axis gimbal system in discussion consists of two rigid bodies free to rotate relative to each other. Gimbal-fixed and Platform-fixed co-ordinate systems, $\{x_g, y_g, z_g\}$ and $\{x_p, y_p, z_p\}$ (frames G and P) are attached to the gimbals and rotate with them. Frame B, $\{x_b, y_b, z_b\}$, is attached to, and rotates with the base on which the gimbals are mounted. It follows then, that equation (3) can be used to develop the general equations of motion for the two-axis gimbal system as defined in Figure 1 above. The platform will first be evaluated before evaluating the yaw-gimbal.

a) Platform Equation of Motion

If the platform is suspended from its principal axes, the assembly has a tensor of inertia, \bar{I}_p , and an angular rate, $\bar{\omega}_p$, such that:

$$\bar{I}_p = \begin{bmatrix} I_{xxp} & 0 & 0 \\ 0 & I_{yyp} & 0 \\ 0 & 0 & I_{zyp} \end{bmatrix}$$

And,

$$\bar{\omega}_p = \begin{bmatrix} \omega_{xp} \\ \omega_{yp} \\ \omega_{zp} \end{bmatrix}$$

Applying (3), the net external torque on the platform, \bar{T}_p , is given by:

$$\bar{T}_p = \bar{I}_p \cdot \dot{\bar{\omega}}_p + \bar{\omega}_p \times \bar{H}_p$$

This gives the net external torque about the platform, y_g, y_p , axis, T_{yp} :

$$T_{yp} = I_{yyp} \dot{\omega}_{yp} + (I_{xxp} - I_{zyp}) \omega_{xp} \omega_{zp} \quad (4)$$

Equation (4) defines the equation of motion for the platform for its rotation about the y_g, y_p axis.

b) Gimbal Equation of Motion

The gimbal, assumed to be suspended from its principal axes, has a tensor of inertia, \bar{I}_g , and an angular rate, $\bar{\omega}_g$, such that:

$$\bar{I}_g = \begin{bmatrix} I_{xxg} & 0 & 0 \\ 0 & I_{y yg} & 0 \\ 0 & 0 & I_{zzg} \end{bmatrix}$$

And,

$$\bar{\omega}_g = \begin{bmatrix} \omega_{xg} \\ \omega_{yg} \\ \omega_{zg} \end{bmatrix}$$

Applying (3), the net torque on the gimbal, \bar{T}_g , is given by:

$$\bar{T}_g = \bar{I}_g \cdot \dot{\bar{\omega}}_g + \bar{\omega}_g \times \bar{H}_g$$

\bar{T}_g is the net torque about the gimbal, therefore, the external torque applied to the gimbal is given by \bar{T}_{gp} :

$$\bar{T}_{gp} = \bar{T}_g + \bar{L}_{PG}^T \cdot \bar{T}_p$$

If,

$$\bar{T}_{gp} = \begin{bmatrix} T_{xgp} \\ T_{ygp} \\ T_{zgp} \end{bmatrix}$$

Then,

$$\begin{aligned} T_{zgp} = T_{zg} + T_{zp} \cos \theta - T_{xp} \sin \theta = & I_{zzg} \dot{\omega}_{zg} \\ & + (I_{yyg} - I_{xxg}) \omega_{xg} \omega_{yg} \\ & + I_{zzp} \dot{\omega}_{zp} \cos \theta \\ & + \omega_{xp} \omega_{yp} (I_{yyp} \\ & - I_{xxp}) \cos \theta \\ & - I_{xxp} \dot{\omega}_{xp} \sin \theta \\ & - \omega_{yp} \omega_{zp} (I_{zzp} \\ & - I_{yyp}) \sin \theta \end{aligned} \quad (5)$$

The angular rates of the platform in terms of the gimbal are given by:

$$\begin{aligned} \bar{\omega}_p &= \begin{bmatrix} \omega_{xp} \\ \omega_{yp} \\ \omega_{zp} \end{bmatrix} = \bar{L}_{PG} \cdot \bar{\omega}_g \\ &= \begin{bmatrix} \omega_{xg} \cos \theta - \omega_{zg} \sin \theta \\ \omega_{yg} + \dot{\theta} \\ \omega_{zg} \cos \theta + \omega_{xg} \sin \theta \end{bmatrix} \end{aligned}$$

And,

$$\dot{\bar{\omega}}_p = \begin{bmatrix} \dot{\omega}_{xp} \\ \dot{\omega}_{yp} \\ \dot{\omega}_{zp} \end{bmatrix} = \begin{bmatrix} \dot{\omega}_{xg} \cos \theta - \dot{\omega}_{zg} \sin \theta - \dot{\theta} \omega_{zp} \\ \dot{\omega}_{yg} + \ddot{\theta} \\ \dot{\omega}_{zg} \cos \theta + \dot{\omega}_{xg} \sin \theta + \dot{\theta} \omega_{xp} \end{bmatrix}$$

Therefore, substituting for $\dot{\omega}_{xp}$ and $\dot{\omega}_{zp}$ in (5):

$$\begin{aligned} T_{zgp} = & (I_{zzg} + I_{zzp} \cos^2 \theta + I_{xxp} \sin^2 \theta) \dot{\omega}_{zg} \\ & + (I_{zzp} - I_{xxp}) \sin \theta \cos \theta \dot{\omega}_{xg} \\ & + \omega_{xg} \omega_{yg} (I_{yyp} - I_{xxp}) \\ & + \omega_{xp} \omega_{yp} (I_{yyp} - I_{xxp}) \cos \theta \\ & + \omega_{yp} \omega_{zp} (I_{yyp} - I_{zzp}) \sin \theta \\ & + I_{zzp} \dot{\theta} \omega_{xp} \cos \theta + I_{xxp} \dot{\theta} \omega_{zp} \sin \theta \end{aligned} \quad (6)$$

Equation (6) defines the equation of motion for the platform for its rotation about the z_b, z_g axis. The angular rates of the gimbal in terms of the base are given by:

$$\begin{aligned} \bar{\omega}_g &= \begin{bmatrix} \omega_{xg} \\ \omega_{yg} \\ \omega_{zg} \end{bmatrix} = \bar{L}_{GB} \cdot \bar{\omega}_b \\ &= \begin{bmatrix} \omega_{xb} \cos \psi + \omega_{zb} \sin \psi \\ \omega_{yb} \cos \psi - \omega_{xb} \sin \psi \\ \omega_{zb} + \dot{\psi} \end{bmatrix} \end{aligned}$$

$$\begin{aligned} \dot{\bar{\omega}}_g &= \begin{bmatrix} \dot{\omega}_{xg} \\ \dot{\omega}_{yg} \\ \dot{\omega}_{zg} \end{bmatrix} \\ &= \begin{bmatrix} \dot{\omega}_{xb} \cos \psi + \dot{\omega}_{yb} \sin \psi + \dot{\psi} \omega_{yg} \\ \dot{\omega}_{yb} \cos \psi - \dot{\omega}_{xb} \sin \psi - \dot{\psi} \omega_{xg} \\ \dot{\omega}_{zb} + \ddot{\psi} \end{bmatrix} \end{aligned} \quad (7)$$

Equations (4), (6), and (7) define the motion of the double gimbal mechanism in terms of base motions and the external

torques on each gimbal. They are used in gimbal dynamics block shown in Figure 14 of Section IV below.

B. Mechanical Design

The mechanical assembly designed in this project was ultimately required to mount the ETX-90 telescope and facilitate control of its inertial orientation. However, due to budget constraints early in the life of the project, it was decided to perform all initial systems development of the ISP without the purchase of the actual telescope, and to rather design a low-cost camera mounting platform to inertially and dimensionally model the ETX-90 and so facilitate the remainder of the systems being developed within the revised budget. To accomplish this an ETX-90 on loan was first modelled using SOLIDWORKS® and formed part of an assembly designed to facilitate its mounting as the platform of the final ISP. This model is shown below in Figure 3.

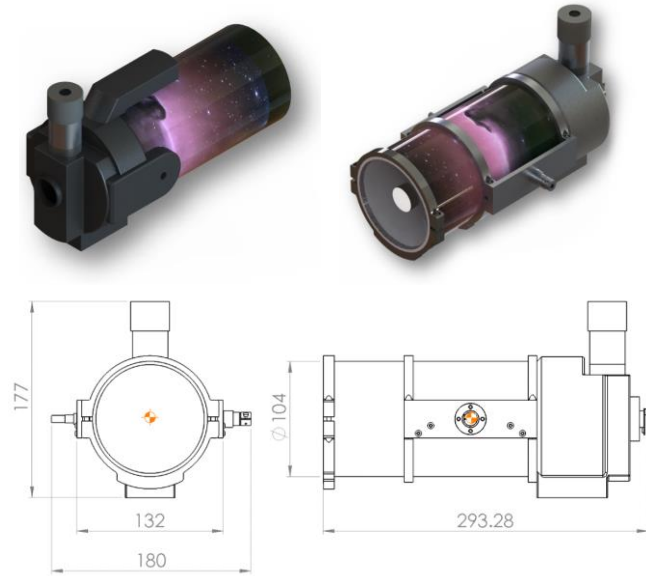


Figure 3: The ETX-90 model (top left), platform assembly (top right), and overall dimensions

This model was then used to establish an estimate of its inertial and geometric properties. The estimated mass of the platform telescope mount was approximately 1.95 kg and had a tensor of inertia, \bar{I}_p :

$$\bar{I}_p = \begin{bmatrix} 0.0049 & 0 & 0.0008 \\ 0 & 0.0165 & 0 \\ 0.0008 & 0 & 0.0162 \end{bmatrix} \text{ kgm}^2.$$

These parameters were then used to inform the design of the low-cost camera mounting system which was used in place of the telescope platform to facilitate systems development and testing over the remainder of the project. This telescope modeler is shown in Figure 4 below.

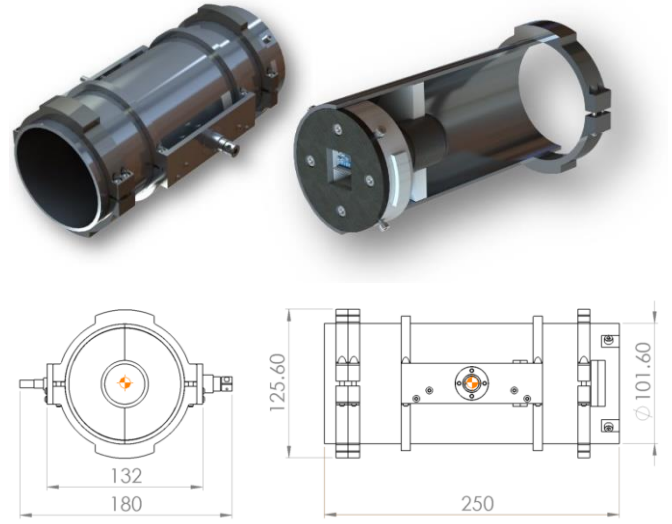


Figure 4: Telescope modeller design

The model can be seen to closely represent the ETX-90 platform, geometrically and inertially, with an estimated mass of 1.90 kg and a tensor of inertia, \bar{I}_p :

$$\bar{I}_p = \begin{bmatrix} 0.0048 & 0 & 0.0009 \\ 0 & 0.0164 & 0 \\ 0.0009 & 0 & 0.0166 \end{bmatrix} \text{ kgm}^2.$$

Following the design of the telescope modeller, the gimbal and mounting stand were designed to support the platform. Care was taken in the design of both the platform and the gimbal to ensure that the assemblies were suspended as close to their principal axes as possible so that the assumption made in the kinematics development regarding zero product of inertia terms was not invalidated. For both the EXT-90 and the telescope modeller, however, the product of inertia terms between the x_p and z_p axes were non-zero, however as these were only approximately 5% of the main moment of inertia terms, I_{yyp} and I_{zzp} , the approximation of these terms to zero was deemed acceptable for the purposes of this project. The final design ultimately had an estimated mass of 6.40 kg and met the desired specification of 9 kg well. This design is shown in Figure 5 below.

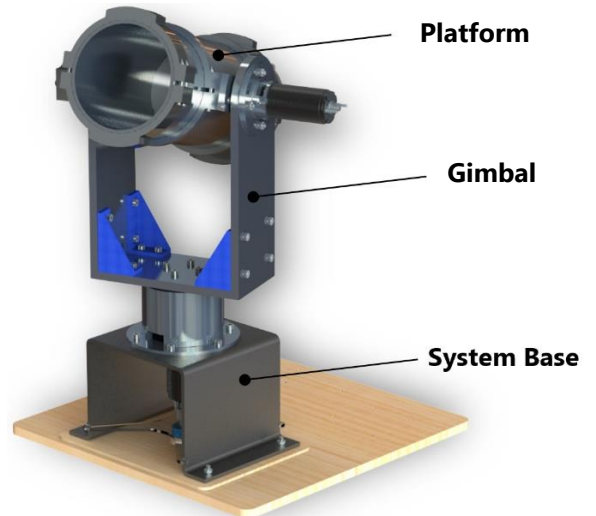


Figure 5: Final design of the ISP and telescope modeller

C. Electrical and Electronic Systems

The electrical and electronic components specified and implemented in this project included the various feedback sensors required to measure the control parameters of the stabilised platform, the electrical systems associated with the actuation of the gimbal and the platform, and the controller hardware used to manage and control the overall system. The feedback sensors implemented are first discussed.

1) Feedback Sensors

The primary control parameter of a stabilised platform is the inertial rotational rate of the sensor requiring stabilisation. In this application the rotational rate LOS of platform is the parameter whose desired value is to be controlled. Measurement of this rate was performed using an InvenSense MPU-9150 MEMS inertial measurement unit (IMU) which was able to measure the inertial rates of up to 250 °/s about three orthogonal axes and output its measurements over an I²C interface. The IMU had suitably low noise and non-linearity properties, high bandwidth and was available at a low cost. This sensor facilitated stabilisation control of the platform to be achieved.

Secondary to the inertial rate sensor, for automatic target tracking to be implemented, a camera sensor was required to be specified. The image from this sensor would provide visual feedback of the target and enable automatic tracking through the stabilisation controller working in conjunction with an image processing algorithm used to locate the target in the camera's FOV. For this project it was decided to use a Raspberry Pi (RPI) Model 3 B computer and Raspberry Pi Camera v1.3 with a modified higher magnification lens to achieve the imaging and target location requirements of the system. The camera sensor's small form factor and the overall low cost of the RPi camera and computer were the dominant factors influencing their use in the project.

The final part of the sensor package used in this ISP were the angle pickoffs used to measure the relative angles between the base and gimbal and the gimbal and the platform. These were chosen to be conductive plastic continuous rotation potentiometers which were also low cost and reliable

but did not add excessive friction to the rotating joints between the gimbals. Figure 6 above shows the implantation of these three sensor types on the ISP assembly.

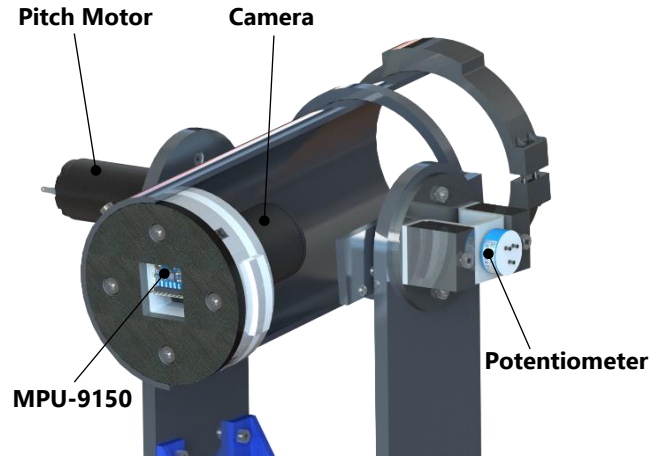


Figure 6: Mounting positions of the system sensors

2) Actuators

Also shown in Figure 6 is the pitch motor. Faulhaber 3257024CR 24V DC motors were chosen for use as the gimbal and platform actuators in this project and were driven by a dual channel, PWM controlled, MOSFET H-bridge. These motors were directly coupled to the mechanics without the use of a gearbox to avoid the backlash induced disturbances and the inherent coupling of the base motion into the ISP gimbals motion when gear drives are used [9].

3) Control Hardware and Architecture

The control hardware chosen for this project included an STM32F0 microcontroller (MCU) which was tasked with interacting with the various sensors and actuators to execute the control laws and communications tasks. In addition, a laptop computer was used to provide a user interface (UI) to facilitate supervisory control of the ISP and perform system datalogging tasks. These controllers were configured, along with the RPi, in a control architecture shown by Figure 7 below.

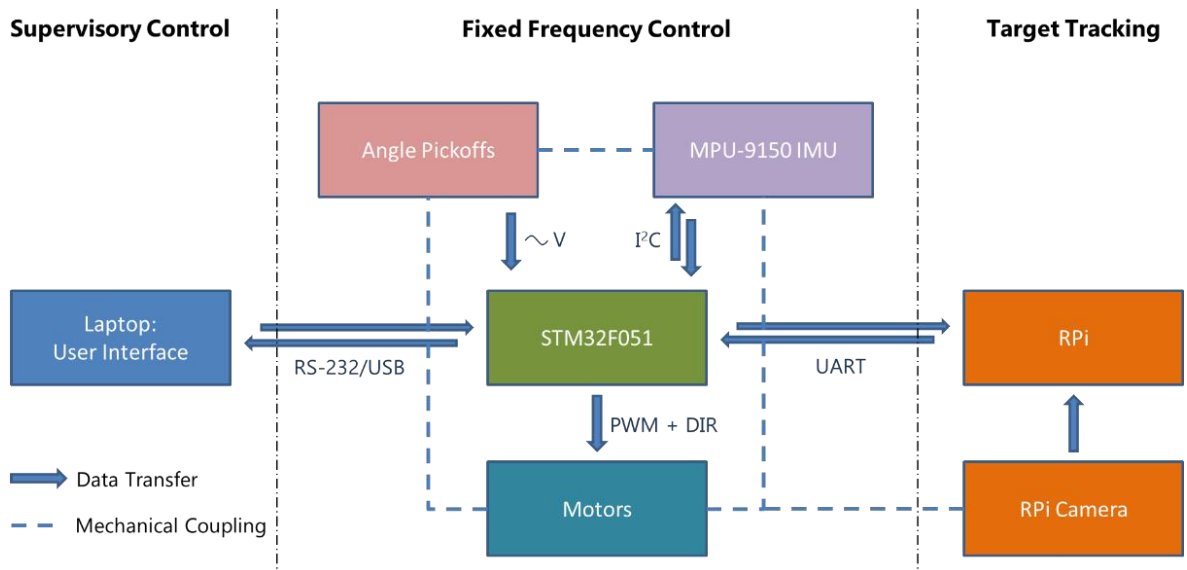


Figure 7: Control hardware configuration

D. Software and Firmware Systems

Three main software/firmware systems were developed for the ISP and used to implement the control architecture shown above: Embedded firmware, written in C, for the STM32 MCU which implemented the control laws and managed system communications tasks, a LabVIEW User Interface (UI) which facilitates supervisory control operations, and an image processing script written in Python 2.7 and based primarily on [10].

The UI facilitated operations such as system start/stop, switching between manual gimbil positioning and automatic tracking and stabilising modes, as well as performing data logging tasks. This UI communicates with the MCU via a bi-directional serial interface over either an RS-232 or USB interface.

The MCU was tasked with reading the angle pickoffs, communicating with the MPU-9150 IMU, managing comms with the RPi which sends target position data to the MCU via a direct pin-to-pin UART connection when the MCU imitates a target data request, and running the control loops, which produce the actuation signals for the yaw and pitch motors which are each controlled using a PWM (speed) and direction signal. Additionally, the MCU is tasked with sending the system runtime data to the UI for data logging.

The RPi is tasked with processing the image produced by the RPi Camera to determine the pixel position of the target centroid, which is then sent to the MCU when the MCU initiates the data request. For this project, a simple colour recognition script was written which returned pixel positions of the centroid of the largest instance of the configured colour. This enabled laboratory testing of the system to occur easily with simulated targets and for simple reconfiguration to recognise the white Moon on the dark background of the night sky to be possible.

IV. SYSTEM SIMULATION AND CONTROLLER DESIGN

Following the systems development of the components of this project's ISP, this section describes the design of the various controller algorithms implemented on the control hardware. Namely, these include manual position controllers for the yaw and pitch channels, stabilisation controllers, and finally tracking controllers for the two channels. Together, these control loops facilitate the control of the ISP such that its orientation and motion may be controlled to a desired state under various operating conditions.

All controllers developed for the ISP were chosen to be classical controllers of type P or PI with compensation. Although modern and non-linear control methods have been shown to achieve superior stabilisation performance, classical controllers were chosen due to the prevalence of their use in the development of stabilised platforms [3], [9], [11]. Additionally, as this project represented the initial systems development of this ISP, classical controllers were the logical starting point for the development of its control system. All controllers designed in this section were determined using the Bode technique and system responses under linear and specific saturated operating conditions representative of the expected operating environment of the ISP.

A. Manual Position Controllers

The manual position controllers serve the purpose of facilitating control of the initial orientation of the telescope before automatic target tracking and stabilisation are initiated. These servo loops on both the yaw and pitch channels made use of compensated PI controllers to actuate the gimbal motors and operated on feedback signals provided by the yaw and pitch angle pickoff potentiometers. The form of the block diagram used to model each channel of the system in this mode is shown by Figure 10. This diagram also shows the motor model used for all control loops designed here and indicates the use of a *STICLIM* function to calculate the frictional moment opposing the motion of the gimbal. *STICLIM* uses a combination of Coulomb and viscous friction and defined limits on angular position to calculate the frictional moment of the system.

These, and the other controllers discussed here, were designed in the continuous s-plane before being transformed to the z-plane using the bilinear transformation and implemented on the MCU using difference equations. The controllers took the form shown in Figure 8 below and ran at a sampling rate of 1 kHz:

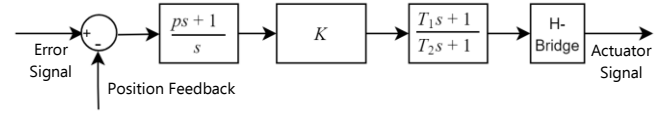


Figure 8: Manual position controllers

Where p is the time constant of the PI controller, K is the controller gain, and T_1 and T_2 are time constants of the compensator zero and pole. The step tracking response of these controllers is shown in Figure 9 below.

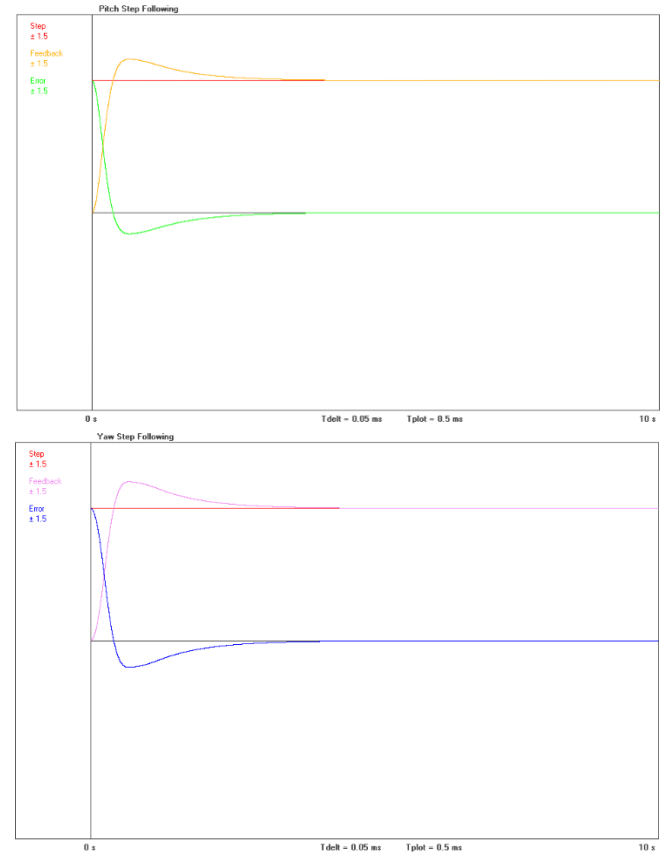


Figure 9: Step response of the manual position controllers

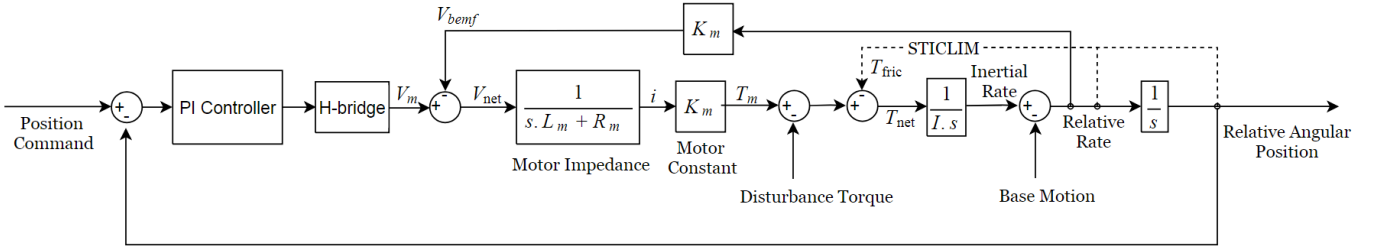


Figure 10: Manual position loop block diagram

B. Stabilisation and Tracking Controllers

Following the design of the manual position controllers, the tracking and stabilisation controllers were designed which facilitate gimbal control whilst the automatic mode is enabled. Typically, an ISP control system consists of two loops per axis configured in a cascade control structure. The outer loop is a low-frequency tracking loop used to keep the sensor pointing toward the target. It also has the objective of removing low-frequency parallax motion between the camera or telescope and the target, and any possible drift in the rate loop. The inner loop is a high-frequency stabilisation loop used to control LOS rate and account for high-frequency disturbances [3], [9]. Figure 14 shows the overall system model block diagram used for the design of these controllers. In that figure, the gimbal dynamics block implements the kinematic relationships between base motions and consequent external disturbance torques applied to the gimbals. The target tracker block includes the relevant mathematical model required to calculate the yaw and pitch tracking errors from the inertial position of the target and the current inertial orientation and rates of the ISP. The yaw and pitch tracking controllers were modelled as shown by Figure 11 below.

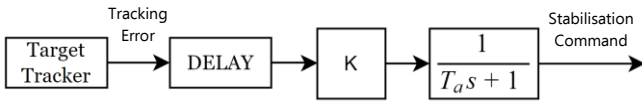


Figure 11: Tracking controllers

P controllers with a compensator with a single pole causing a phase lag at frequencies above 10 Hz were implemented as the tracking controllers. The delay block above models the delay caused by the image processing algorithm in identifying the target in the FOV. These controllers showed no resonance and had a low bandwidth of approximately 1 Hz which, however, was sufficient for the application as celestial bodies move slowly across the sky at frequencies far lower than 1 Hz. The yaw and pitch

stabilisation controllers were modelled as shown in Figure 12 below.

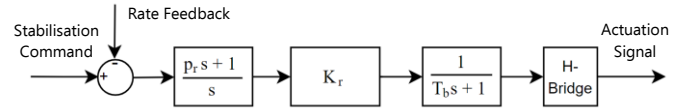


Figure 12: Stabilisation controllers

PI controllers with a compensator with a single pole causing a phase lag at frequencies above 150 Hz were implemented as the stabilisation controllers. Experimental testing during the project revealed that the dominant disturbances expected to be incurred to the ISP if mounted on a moving vehicle would be at frequencies less than 5 Hz with a peak amplitude of less than 0.05 rad/s. Therefore, the integrator component of the controller was required in order to ensure adequate low frequency disturbance rejection performance. These loops had bandwidths of approximately 38 Hz and resonance peaks of less than 3 dB. The figure below shows the step response of the ISP to the command positions, $\theta = 45^\circ, \psi = -45^\circ$. This was done by setting the target position to $\{x_i, y_i, z_i\} = \{1000, -1000, -1414.2\}$.

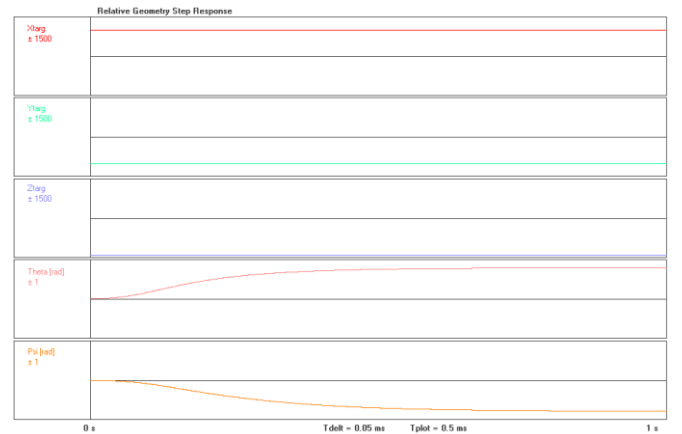


Figure 13: Tracking step response

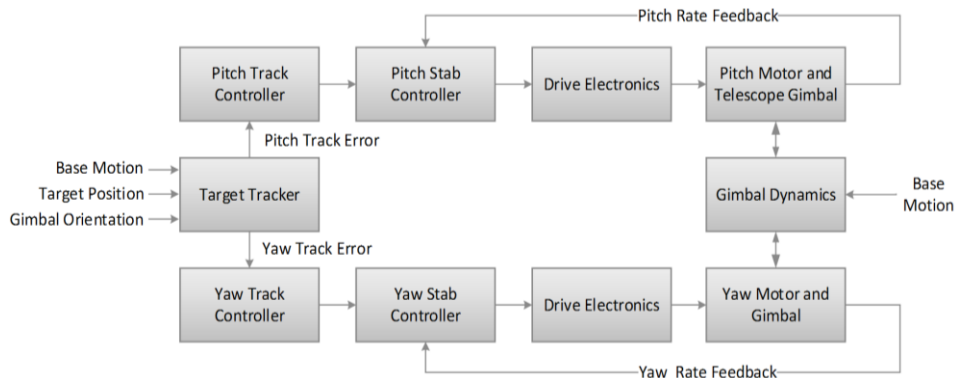


Figure 14: System model block diagram

As previously stated, the main purpose of the stabilisation controller is to attenuate disturbances incurred to the sensor LOS. The primary source of these disturbances is the base motion of the host vehicle to which the ISP is mounted. Base motion disturbance coupling is dependent on the orientation of the ISP gimbals and is at its worst case when $\theta = 45^\circ$, $\psi = -45^\circ$. Figure 15 below illustrates the simulated performance of the ISP system at attenuating 0.25 rad/s base motion disturbances at frequencies up to 5 Hz in this position.

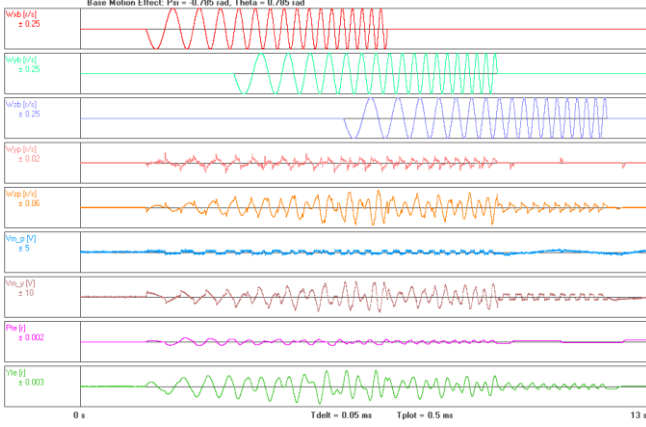


Figure 15: Base motion attenuation of 0.25 rad/s signals

In the figure above, the first three plots are frequency swept sinusoids modelling a base motion applied to the system. Plots 4 and 5 indicate the LOS rates about the y_p and z_p axes. The base motions of 0.25 rad/s peak are attenuated to about 0.01 rad/s peak in LOS pitch and about 0.05 rad/s peak in LOS yaw. Plots 6 and 7 show the motor voltages over the test and the final two plots indicate the pitch and yaw tracking error respectively.

V. MODEL VERIFICATION

The simulated model above was verified experimentally as the final phase of the project. The simulated tracking step responses were compared to the implemented system's responses by comparing the error signals of the yaw and pitch tracking controllers of the simulation to the experimentally measured error signals of each channel's controller in response to control step commands. This is shown for the yaw channel in Figure 16 and Figure 17 below, where Ytc is the yaw tracking command, and Yte is the error signal.

The setpoint chosen in these figures was equal to the angles (in rad) between the target and the LOS of the camera at the limits of its FOV for each channel. On the physical system setup in this position, the system was then set to the Automatic mode and allowed to actuate the gimbals such that the target was placed onto the LOS of the camera. The pixel positions of the target centroid were recorded during this test and converted to angle measurements from the LOS of the sensor to the target using a linear approximation relating pixel count to angle which was based on the properties of the camera lens used. The image processing algorithm achieved an average framerate of 17 frames per second and the quantisation effect on the physical test signal in response to this is clearly evident in Figure 17, however this does not impair the performance of the controller overly much: In these figures it can be seen that on the application of the step command both the simulated and implemented controllers

overshoot the command by approximately 8 % before settling to the command after approximately 1.5 s. The simulation shows marginally greater oscillation than the physical test, however, it is hypothesised that the additional damping is due to disturbance torques exerted on the ISP by cable flexure which was not modelled in the system simulation. Overall it was concluded that the tracking controllers simulated performance matched the measure performance well.

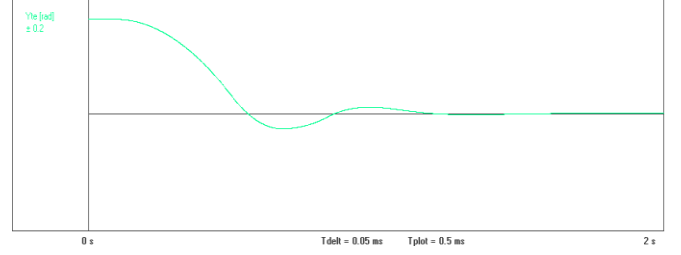


Figure 16: Simulated step tracking controller error on the yaw channel

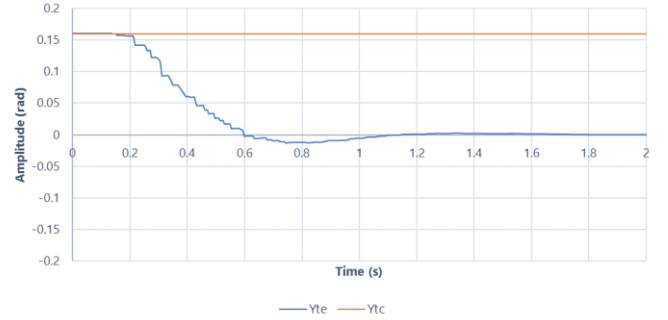


Figure 17: Measured step tracking controller error on the yaw channel

Base motion isolation (BMI) of the ISP is defined below.

$$BMI = 20 \log \left| \frac{\text{Amplitude } \omega_{np}}{\text{Amplitude } \omega_{nb}} \right| \quad (9)$$

where $n \in \{x, y, z\}$

BMI was evaluated by applying a base motion to the ISP, which was recorded using an MPU-9150 IMU attached to the system base and recording the LOS rates during the test. Several iterations of the test were repeated with the ISP in various orientations and for various base motion input profiles. Figure 18 below is indicative of the test results for the ISP. It shows the profile of a large base motion applied to the y_b axis and the associated LOS rates about the y_p and z_p axes.

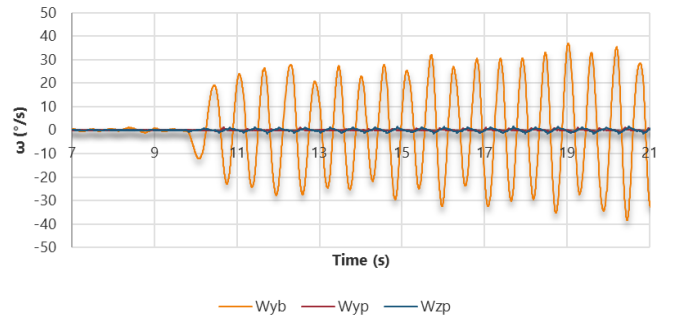
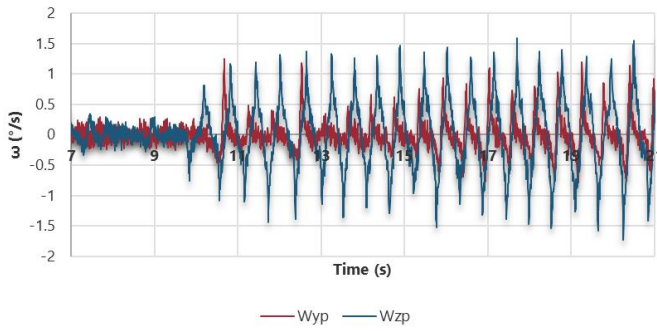


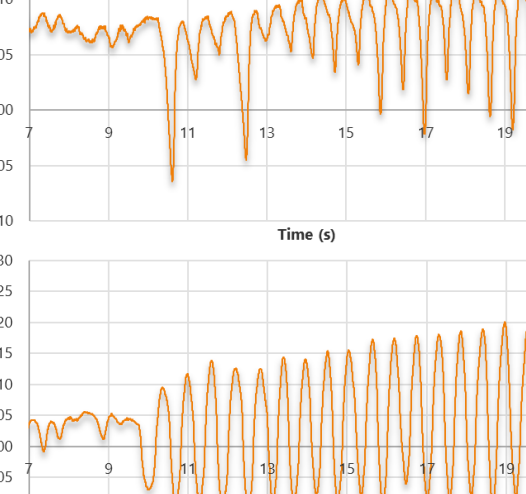
Figure 18: Base motion attenuation of the ISP

The LOS rates in response to the base motion above, are shown in more detail in Figure 19 below.



This disturbance, ω_{yb} in Figure 18, had a median amplitude of approximately 28.93 °/s at 1.5 Hz for positive disturbances about the y_b axis between 11 - 21 s of the test, whilst the median amplitude value of ω_{yp} over the same period was approximately 0.91 °/s. This represents a BMI from ω_{yb} to ω_{yp} of -30.0 dB. For the same period, the median amplitude of ω_{zp} was approximately 1.39 °/s resulting in a cross-axis BMI from ω_{yb} to ω_{zp} of approximately -26.3 dB. The validity of the simulation model for base motion tests was then established by repeating the experimental test conditions in the simulation environment. For the test example shown above, the simulation was run using a sine wave base motion of amplitude 28.93 °/s at 1.5 Hz about y_b . The result of this test is shown in Figure 20 below where it can be seen that the simulation shows a similar response to the hardware results above: Inertial rate, ω_{yp} , peaks at 0.017 rad/s or 0.97 °/s which matches the test data within 8 %, whilst ω_{zp} , has a peak value (disregarding the initial peak) of 0.025 rad/s or 1.43 °/s which matches the test results within 3 %.

An approximate measure of angle jitter was evaluated for these tests by integrating the LOS rate signals about relevant axes. Figure 21 below shows the results of integrating the ω_{yp} and ω_{zp} signals in Figure 18.



The figure consists of two vertically stacked line plots. The top plot shows 'Pitch Jitter (rad)' on the y-axis (ranging from -0.0010 to 0.0015) against 'Time (s)' on the x-axis (ranging from 7 to 21). The bottom plot shows 'Yaw Jitter (rad)' on the y-axis (ranging from -0.0015 to 0.0030) against 'Time (s)' on the x-axis (ranging from 7 to 21). Both plots show a blue line representing the jitter signal over time. The Pitch Jitter signal starts around 0.0007 rad, fluctuates, and then shows a sharp negative spike to approximately -0.0007 rad at 11 seconds. The Yaw Jitter signal starts around 0.0004 rad, fluctuates, and then shows a sharp negative spike to approximately -0.0007 rad at 11 seconds. Both signals exhibit high-frequency oscillations after 11 seconds.

It can be seen from the test results above that pitch jitter in response to a large base motion at a frequency within the expected operating region was approximately 1.25 mrad, whilst yaw jitter was approximately 1.70 mrad from the mean positions of the signals. Overall, the performance achieved by the ISP across several tests is summarised by Table 1 below.

Metric	Pitch Channel	Yaw Channel
BMI with disturbance axis aligned with attenuation axis	-34.4 dB (1.1 rad/s at ~2 Hz disturbance)	-31.5 dB (1.2 rad/s at ~2.5 Hz disturbance)
BMI with disturbance axis cross-coupled with attenuation axis	-30.0 dB (0.5 rad/s at ~1.5 Hz disturbance)	-26.3 dB (0.5 rad/s at ~1.5 Hz disturbance)
Maximum tracking rate	0.75 rad/s	0.99 rad/s
Maximum track overshoot	11.6 mrad	12.3 mrad
Maximum track step settling time	1.5 s	1.5 s
Maximum dynamic jitter	2.35 mrad	2.52 mrad
Maximum stationary jitter	1.0 mrad	0.5 mrad

It can be seen from the test results above that BMI for the ISP for disturbances which are aligned with the attenuation axis are of the order of -32 dB which matches well with other platforms developed in contemporary literature [12], [13]. In addition, system jitter can also be seen to approximately be limited to the initial specification.

VI. CONCLUSION

Overall, a two-axis stabilised platform was developed capable of stabilising a telescope modeller camera mount and achieving automatic tracking of the Moon. With reference to the main system specifications introduced earlier in this document, all major specifications were approximately met apart from the maximum allowable tracking error of 0.25 mrad. Tracking error achieved was 0.5 mrad and was due to

the RPi computer not being able to process images of a high enough resolution to meet the specifications at a rate suitable for the tracking loops of the ISP control system, therefore requiring a limitation to be placed on the image resolution meaning that a 0.25 mrad error on the tracking system was not detectable to the system. In addition, the project ran marginally over budget with approximately R6700.00 being spent on development rather than the initial target of R5000.00.

However, automatic target tracking was achieved, and an expansion friendly mechanical design was implemented which can facilitate the inclusion of the Meade ETX-90 telescope easily. Classical controllers were designed and tested using a telescope modeller which inertially and geometrically modelled this telescope, and therefore it is not expected that the control algorithms will require much adjustment to effectively stabilise the ETX90 once it has been included. This system was experimentally shown to achieve similar performance to other ISPs developed for research purposes and to perform closely to the manner predicted by the simulation developed.

REFERENCES

- [1] A. K. Rue, "Precision Stabilization Systems," *IEEE Trans. Aerosp. Electron. Syst.*, vol. AES-10, no. 1, pp. 34–42, 1974.
- [2] H. Khodadadi, M. R. J. Motlagh, and M. Gorji, "Robust control and modeling a 2-DOF inertial stabilized platform," *InECCE 2011 - Int. Conf. Electr. Control Comput. Eng.*, pp. 223–228, 2011.
- [3] J. M. Hilkert, "Inertially stabilized platform technology: Concepts and principles," *IEEE Control Syst. Mag.*, vol. 28, no. 1, pp. 26–46, 2008.
- [4] B. Ekstrand, "Equations of motion for a two-axes gimbal system," *IEEE Trans. Aerosp. Electron. Syst.*, vol. 37, no. 3, pp. 1083–1091, 2001.
- [5] H. D. Mouton, "Ondersoek Na Die Hoëprestatiebeheer en Vergelykende Vermoë van Verskillende Tipes Missielvolgkoppe Ten Opsigte van Stabilisasie en Volgakkuraathede," Potchefstroomse Universiteit vir Christelike Hoer Onderwys, 1993.
- [6] F. N. Barnes, "Stable Member Equations of Motion for a Three-Axis Gyro Stabilized Platform," *IEEE Trans. Aerosp. Electron. Syst.*, vol. AES-7, no. 5, pp. 830–842, 1971.
- [7] A. K. Rue, "Stabilization of Precision Electrooptical Pointing and Tracking Systems," no. 5, 1969.
- [8] J. L. Meriam and L. G. Kraige, *Engineering Mechanics Dynamics*, 6th ed. John Wiley & Sons, Inc., 2008.
- [9] M. K. Masten, "Inertially stabilized platforms for optical imaging systems," *IEEE Control Syst. Mag.*, vol. 28, no. 1, pp. 47–64, 2008.
- [10] A. Rosebrock, "Increasing Raspberry Pi FPS with Python and OpenCV," 2015. [Online]. Available: <https://www.pyimagesearch.com/2015/12/28/increasing-raspberry-pi-fps-with-python-and-opencv/>. [Accessed: 30-Mar-2018].
- [11] Z. Hurak and M. Rezac, "Image-based pointing and tracking for inertially stabilized airborne camera platform," *IEEE Trans. Control Syst. Technol.*, vol. 20, no. 5, pp. 1146–1159, 2012.
- [12] Young Shin Kwon, Hong Yeon Hwang, and Yun Seok Choi, "Stabilization Loop Design on Direct Drive Gimbaled Platform With Low Stiffness and Heavy Inertia," in *2007 International Conference on Control, Automation and Systems*, 2007, pp. 320–325.
- [13] S. Li and M. Zhong, "High-Precision Disturbance Compensation for a Three-Axis Gyro-Stabilized Camera Mount," *IEEE/ASME Trans. Mechatronics*, vol. 20, no. 6, pp. 3135–3147, 2015.